Abstract:

Reflectance confocal microscopy (RCM) can be an additional tool to dermoscopy for diagnosis of "early / micro" lesions of basal cell carcinoma (BCC). "Dark area" surrounding tumor-cell nests with star formation is a unique, important sign.

Key words: basal cell carcinoma, dermoscopy, reflectance confocal microscopy, nevoid basal cell carcinoma

Reflectance confocal microscopy (RCM) has been introduced recently in clinical dermatology[1-8], including *in vivo* imaging of BCCs[5-7]. We investigated if "early /or micro" lesions of BCC could be accurately diagnosed by RCM combined with dermoscopy.

Materials and methods:

Five BCC lesions from four patients were investigated by dermoscopy and subsequently by *in vivo* or *ex vivo* RCM, i.e., RCM examination before and after surgical excision respectively. Dermoscopy followed the two-step method of the "consensus net meeting on dermoscopy 2000" [9, 10], using commercially available DermoGenius basic (LINOS, Königsallee, Germany) and digital camera (Coolpix 3600, Nikon Corporation, Tokyo, Japan). Confocal imaging was performed using a commercially available RCM with a near-infrared (830nm Diode) laser (Vivascope 1500, Lucid Inc., Rochester, NY). Five % acetic acid was used to enhance images[11](Fig B, F).

Results:

Five BCC lesions were investigated (Table).

Case 1: A brown plaque (10 x 8 mm) with "pearly border" (Fig 1 A). *Ex vivo* RCM revealed the following morphologic features unique to pigmented BCC. Firstly, it could elucidate the individual tumor-cell nests, and revealed bright, oval satellite-like structures, which represented aggregates of melanin pigments or melanocytes, locating in the nests of tumor cells (Fig 1-B, C). The dermal stromas surrounding tumor-cell nests (parenchyma) often showed oval reflecting

bodies with some bright-colored structures which represented melanophages (Fig 1 B). Secondly, the spoke-wheel areas of dermoscopy correlated well with tumor-cell nests on RCM (Fig 1 D, E), which, however, revealed peripheral-dark area surrounding the tumor cell nests (Fig 1 B, E). Thirdly the "spoke" of spoke-wheel areas of dermoscopy (Fig 1 D) was also shown by RCM (Fig 1E) and confirmed by vertical HE sections (Fig 1 G). The palisading and cleft formation on HE sections (Fig 1 G) correlated well with palisaded bright and peripheral dark areas on cross-sectional view of *ex vivo* RCM (Fig1 F).

Case 2: A flat erythematous, slightly scaly lesion (10 mm in diameter) with irregular border (Fig 2A). *Ex vivo* RCM could visualize global-tumor structures that was hardly detected by dermoscopy (Fig 2B, C).

Case 3: A multiple small, round pigmented BCC lesions on whole body from a nevoid BCC syndrome patient. Dermoscopy of an oval brown lesion (2 mm in diameter) on right cubital fossa could detect multiple blue-gray dots or globules and spoke-wheel like areas by digital magnification (Fig 2 D). Dermoscopy of another pigmented lesion (2 mm in diameter) on right back revealed two spoke-wheel areas by digital magnification (Fig 2 E). However, it was *in vivo* RCM that visualized easily not only spoke-wheel like lesions but also tumor cell nests. Besides, *in vivo* RCM could show tumor-cell nests (parenchyma) surrounded by dark areas (Fig 2 F), and bright areas of tumor periphery with "star formation" (Fig 2 G).

Case 4: A lesion with ulceration and telangiectasia from a Caucasian male (Fig 2 H). *Ex vivo* RCM could visualize the tumor parenchyma surrounded by dark areas (Fig 2 I).

Discussion:

Dermoscopy is a noninvasive optical strategy for imaging skin-tumors.[1] We found that RCM represents another imaging technology with greater resolution and contrast up to a depth of 350 μm, providing skin imaging in real time at a resolution almost equal to that of conventional microscopes[1, 2]. RCM would help us to avoid unnecessary surgery by differentiating *in vivo* pigmented BCCs from other pigmented tumors and detecting "early/micro" BCC as small as 2 mm with images comparable to those of "common" BCC (larger than 5mm). RCM could visualize the peripheral dark areas surrounding tumor-cell nests (parenchyma) and the palisaded tumor cells in "early" / micro-" lesions. RCM could also identify the extent of horizontal infiltration of BCCs, which could not be recognized by dermoscopy (Fig 2 G, I). However, RCM could not define accurately the depth of tumor invasion, which is the limitation of this technology. The tumor depth can accurately be diagnosed histologically. Peripheral dark areas of decreased signal between tumor parenchyma and adjacent dermal stroma, which were reported by Vinh Q *et al*,[12] were found to represent clefts accumulated with mucinous substances in HE sections.[13] Lacunae, which are regarded as a fixation artifact, but can also be observed on cryostat section[13], have been thought to correspond to "dark areas" by *in vivo* RCM (Fig 2 F, G). Our study of *in vivo* and *ex vivo* RCM confirmed that these areas represent loose stroma accumulated with mucinous substances on HE sections. These findings were not seen by RCM in any other skin tumors, e.g., malignant melanoma, dermatofibroma, soft fibroma, trichoepithelioma, seborrheic keratosis, dermatofibrosarcoma protuberance, Merkel cell carcinoma and solar lentigo (data was not shown). Thus, RCM finding

of "dark areas" surrounding tumor parenchyma is a unique, diagnostic sign for "early" / micro-" lesion of BCC. In our case #2 and #4, dermoscopy revealed ulceration and arborizing vessels, but not dots or globules. RCM, however, demonstrated clearly bright tumor parenchyma and dark peripheral areas (Fig 2 C-1). RCM could well demonstrate tumor margin of pigmented / non-pigmented BCC, but there is a limitation to visualize the entire tumor border, though we could identify global tumor structure less than 3 mm as in case #3 (Fig 2F). The current RCM technology can only show the limited lesions of full-size XY-maps and any lesion larger than 3.0- 3.5 mm will not 'fit' on the screen in its entirety. In "early / micro-" lesions of BCC, dermoscopy allowed us to visualize the multiple blue-gray dot or globules and spoke-wheal areas by magnification with digital camera (Fig 2 D, E). However, RCM could easily visualize spoke-wheel like structures which we called "star formation" (Fig 2 G). Hence, the combined observation of dermoscopy and RCM is useful for diagnosing "early / micro" lesions of BCC that dermoscopy alone can hardly detect. RCM identifies not only the surface structure of BCC but also their inside structure, i.e., "dark areas" surrounding the tumor-cell nests. These RCM features appear to diagnostic for BCCs, specifically for "early / micro-" lesions. Their sensitivity and specificity, however, need to be tested by additional large studies.

References

1. Ruocco E, Argenziano G, Pellacani G, Seidenari S. Noninvasive Imaging of Skin Tumors. Dermatol Surg 2004; 30: 301-310.

2. Rajadhyaksha M, Gonzales S, Zavislan JM, Anderson RR. In vivo confocal scanning laser microscopy of human skin: Advances in instrumentation and comparison with histology. J Invest Dermatol 1999; 113: 293-303.

3. Busam KJ, Charles C, Lee G, Halpern AC. Real-time, in vivo confocal reflectance microscopy of basal cell carcinoma. J Am Acad Dermatol 2002; 47: 869-74.

4. Rajadhyaksha M, Grossman M, Esterowitz D, Webb RH, Anderson RR. In vivo confocal scanning laser microscopy of human skin: melanin provides strong contranst. J Invest Dermatol 1995; 104: 946-52.

5. Nori S, Rius-Diaz F, Cuevas J, Goldgeier M. Sensitivity and specificity of reflectance-mode confocal microscopy for in vivo diagnosis of basal cell carcinoma: a multicenter study. J Am Acad Dermatol 2004; 51: 923-30.

6. Sauermann K, Gambichler T, Wilmert M, Rotterdam S. Investigation of basal cell carcinoma [correction of carcionoma] by confocal laser scanning microscopy in vivo. Skin Res Technol 2002; 8: 141-7.

7. Gonzalez S, Tannous Z. Real-time, in vivo confocal reflectance microscopy of basal cell carcinoma. J Am Acad Dermatol 2002; 47: 869-74.

8. Charles CA, Marghoob AA, Busam KJ, Clark-Loeser L. Melanoma or pigmented basal cell carcinoma: a clinical-pathologic correlation with dermoscopy, in vivo confocal scanning laser microscopy, and routine histology. Skin Res Technol 2002; 8: 282-287.

9. Rajadhyaksha M, Menaker G, Flotte T, Dwyer PJ, Gonzalez S. Confocal examination of nonmelanoma cancers in thick skin excisions to potentially guide mohs micrographic surgery without frozen histopathology. J Invest Dermatol.2001;117:1137-39.

10. Argenziano G, Soyer HP, Chimenti S, Talamini R. Dermoscopy of pigmented skin lesions: results of a consensus meeting via the Internet. J Am Acad Dermatol 2003; 48: 679-93.

11. Menzies SW, Westerhoff K, Rabinovitz H, Kopf AW. Surface microscopy of pigmented basal cell carcinoma. Arch Dermatol 2000; 136: 1012-1016.

12. Chung VQ, Harmsci MP, Dwyer PJ, Nehal KS, Rajadhyaksha M, Menaker GM, Charles C, Jiang SB. Use of ex vivo confocal scanning laser microscopy during Mohs surgery for nonmelanoma skin cancers. Dermatol Surgery 2004; 30: 1470-1478.

13. Kirkham N. Tumors and cysts of the epidermis. In: Lever's Histopathology of the Skin. 9th edition. Elder DE, Elenitsas R, Jaworsky C, Johnson B Jr, editors. Lippincott Williams & Wilkins. 2005; p.842.

Figure legends

Figure 1.

A. Dermoscopic view of case 1, showing multiple blue-gray globules (blue arrows), arborizing vessels (white arrows), spoke-wheel areas (white arrow-heads) and maple-leaf like areas (red arrows). (scale bar: 1.0 mm). An insert shows a brown plaque of BCC (10× 8 mm) with "pearly border".

B-C. Comparison of *ex vivo* RCM and histopathological view of BCC lesion shown in Fig 1-A, which consists of tumor-cell nests (parendryma) with irregular border.

B. Vertical *ex vivo* RCM view of the peripheral margin of tumer-cell nests which consists of palisading arrangement and irregular club-like tumor invasion, and oval or satellite-like structures with bright-reflectance, representing clumps of melanin pigments or melanocytes (scale bar: 50μm). Five % acetic acid was used to enhance images.

C. Horizontal *ex vivo* RCM view of irregular tumor parenchyma with peripheral bright-reflecting area, showing the palisading and dark areas. (scale bar: 100 μm)

D. Dermoscopic view of spoke-wheel areas of irregularly shaped, tumor-cell nests shown in Fig1-A.

E. *Ex vivo* RCM view of Fig 1-D showing peripheral dark areas (arrow heads) of tumor margins. (scale bar: 500μm)

F. Vertical *ex vivo* RCM view for a cross-section of spoke, showing bright areas (arrow heads) surrounded by dark areas (arrow) that correlate well with HE section (scale bar: 50μm). Five % acetic acid was used to enhance images.

G. Vertical HE section of spoke revealing oval tumor parenchyma surrounded by the palisading arrangement and cleft formation×400.

Figure 2

A: Dermoscopy of case 2 revealing ulcer (arrows) and arborizing vessels (arrow head), but without dot/globules. (scale bar: 1.0 mm) An insert shows an atrophic BCC Lesion (scale bar: 10 mm).

B, C-1: Comparison of horizontal dermoscopic (B) and *ex vivo* RCM (C) views reveal ing bright-colored, tumor-cell nests surrounded by dark areas (arrow head). (scale bar: 500μm)

C-2: Horizontal *ex vivo* RCM view of irregular tumor parenchyma with peripheral bright-reflecting area, showing the palisading and dark areas(scale bar: 100μm).

D: Dermoscopy view of case 3 with multiple blue-gray globules (arrow heads) and spoke-wheel like area (arrow). An insert shows a 2-mm-sized, brown papule of BCC (scale bar: 200μm).

E: Dermoscopy of case 3 with digital magnification showing two spoke-wheel areas (arrows). An inset shows a 2-mm sized, brown papule of BCC (scale bar: 500μm).

F: Horizontal *in vivo* RCM of case 3, revealing spoke-wheel areas of dermoscopy (E), which correlate to tumor-cell nests with irregular borders surrounded by dark-gray areas of *in vivo* RCM. (scale bar: 500μm)

G: *In vivo* RCM view revealing star-shaped, tumor margin which is surrounded by dark-gray areas and peripheral bright portions. A spoke-wheel like structure which we called "star formation". (scale bar: 100μm)

H: Dermoscopy of case 4, revealing ulcer and arborizing vessels, but without dot/globules (scale bar: 5mm). An insert shows a 2-mm- sized, ulcerating BCC with peripheral telangiectasia.

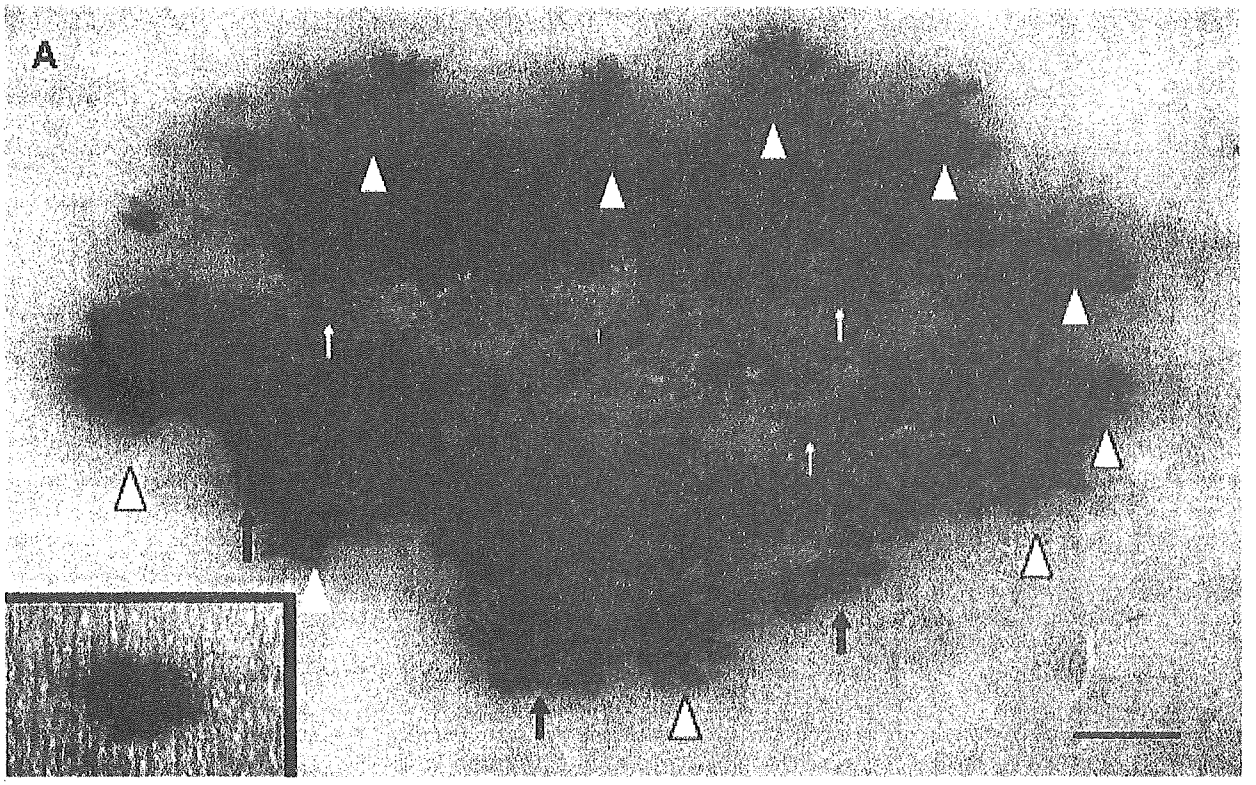
A

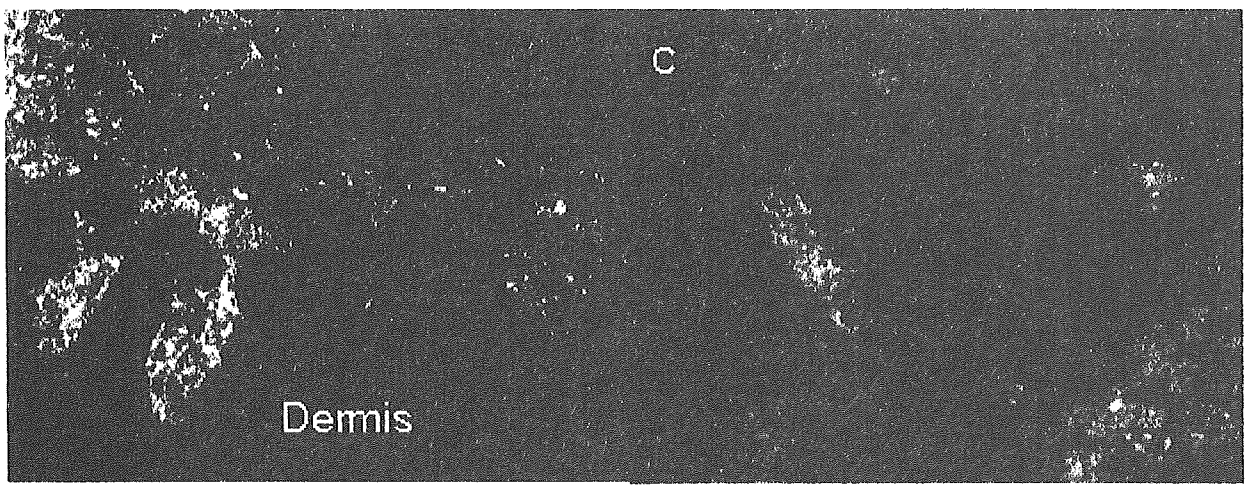
C
Demis

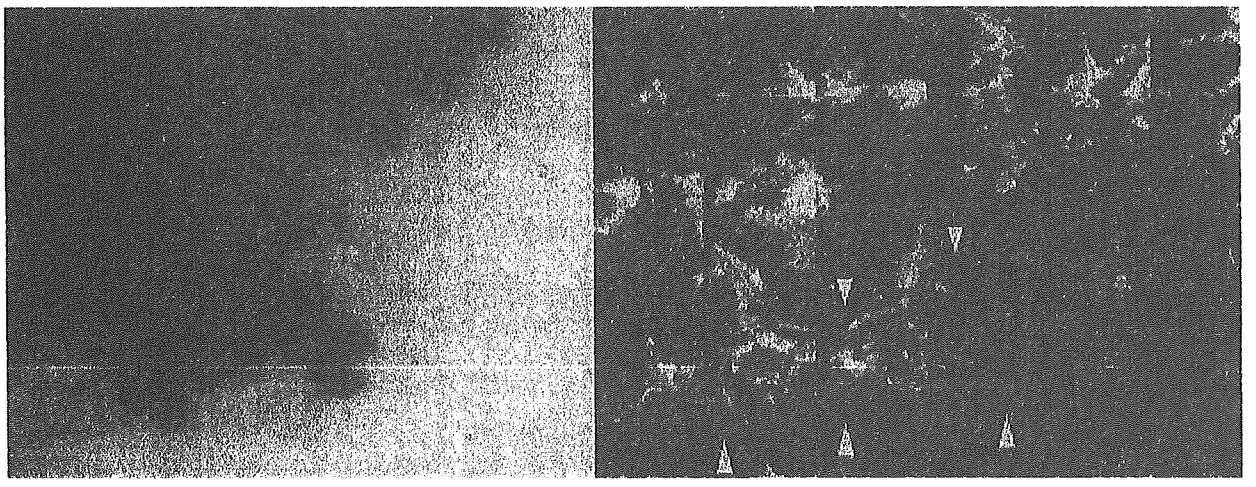

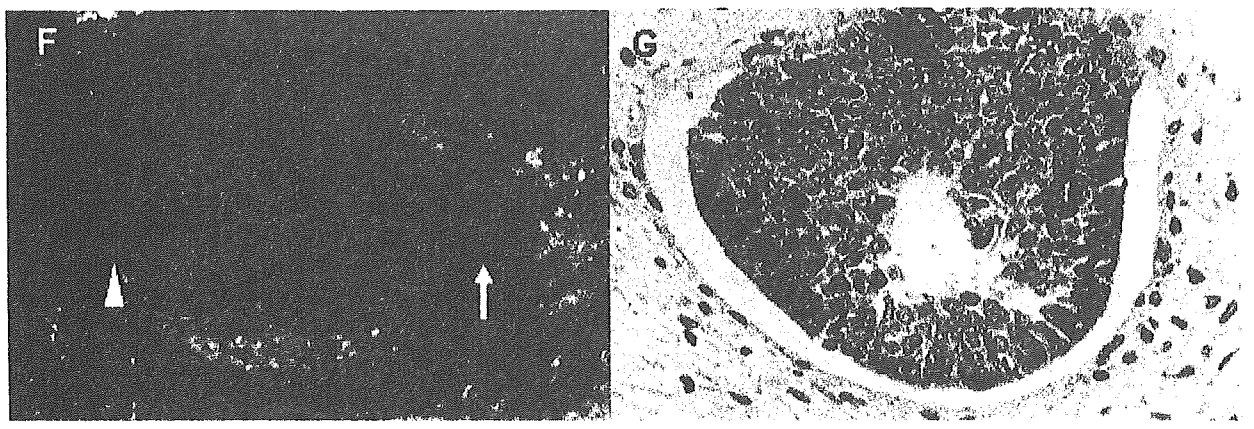
F
G

I: *Ex vivo* RCM of case4, revealing peripheral-dark areas which surround the tumor parenchyma(scale bar: 50μm). The tumor was excised 3 mm free margin from the tumor and processed to ex vivo RCM.

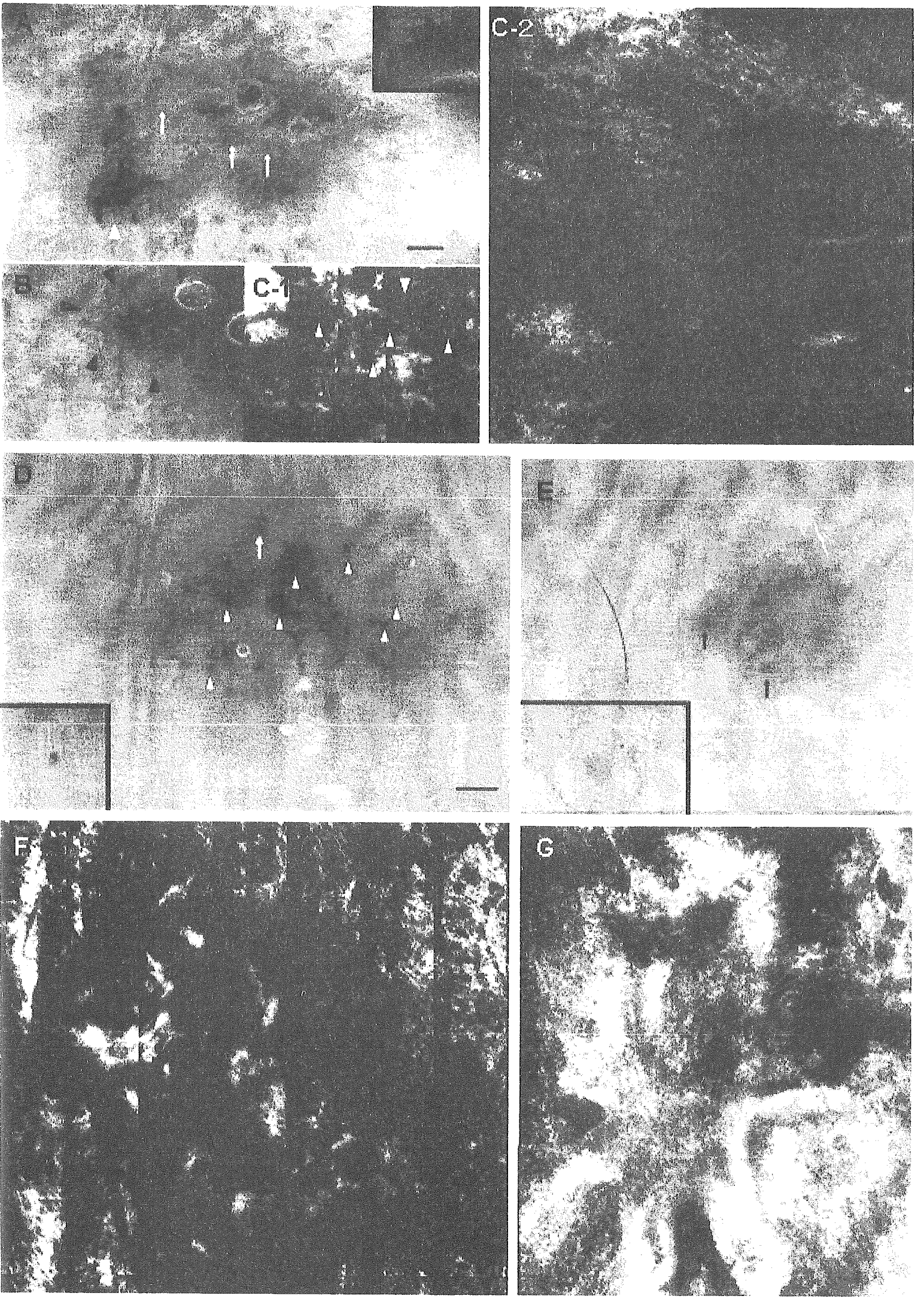
B
C-1
C-2
D
E
F
G

Table: Comparison of dermoscopy and RCM findings

Case & Clinical feature	Dermoscopy	RCM
#1. 80 y.o. male 10x8mm-sized, brown papule with pearly border.	• Multiple blue-gray globules • Arborizing vessels • Spoke-wheel areas • Maple leaf-like areas	• Tumor border with irregular bright areas of palisade arrangement • Dark area surrounding tumor parenchyma
#2. 75 y.o. female 10mm-sized, erythematous papule	• Ulceration • Arborizing vessels	• Depth and invasion of tumor • Dark area surrounding tumor border
#3. 52 y.o. female with nevoid basal cell carcinoma syndrome		
a) 2mm-sized brown papule	• Multiple blue-gray globules • Spoke-wheel--like areas	Not done
b) 2mm-sized, light-brown papule	• Spoke-wheel areas	• Star-shaped, irregular tumor border with bright areas of palisade arrangement • Dark area surrounding tumor border
#4. 49 y.o. male 2mm-sized papule with ulceration and peripheral telangiectasia	• Ulceration • Arborizing vessels	• Star-shaped, irregular tumor border • Dark area surrounding tumor border

An immunosuppressive effect by β-SQAG9 on swine allogeneic skin grafting

Running title: Prolongation of skin allograft survival by β-SQAG9

Akihito Imai[1, 2], Hiroeki Sahara[5], Mika Takenouchi[2], Yoshiteru Yamamoto[1, 2], Yoshitaka Matsumoto[1], Tatsuya Fujita[1], Yasuaki Tamura[2], Nobuyuki Takahashi[5], Shinsei Gasa[3], Kenjirou Matsumoto[6], Keisuke Ohta[6], Fumio Sugawara[6], Kengo Sakaguchi[6], Kowichi Jimbow[4], Takatoshi Yotsuyanagi[1], and Noriyuki Sato[2, 5]

[1]Department of Plastic Surgery, [2]Pathology, [3]Chemistry and [4]Dermatology, Sapporo Medical University School of Medicine, Sapporo, Japan, [5]Marine Biomedical Institute, Sapporo Medical University School of Medicine, Oshidomari, Rishirifuji, Hokkaido, Japan; [6]Department of Applied Biochemical Science, Science University of Tokyo, Noda, Chiba, Japan.

Corresponding author:

Hiroeki Sahara

86 Minato-machi, Oshidomari, Rishirifuji-cho, Hokkaido 097-0101, Japan

Tel & Fax: +81-163-82-1250

e-mail: hsahara@sapmed.ac.jp

Abstract

We previously reported that sulfo-glycolipid, β-SQAG9, possessed immunosuppressive effects, such as inhibition of T cell responses in human allogeneic MLR and skin allograft survival in rat. In this study, we evaluated the immunosuppressive effect of β-SQAG9 by swine allogeneic skin grafting. We used hybrid pigs of about 20kg weight as donor and recipient and divided them into three groups, control, FK506, and β-SQAG9. After transplantation, FK506 and β-SQAG9 was administrated at 0.25mg/kg and 50mg/kg once per day for a week, respectively. In the control group, complete rejection was observed on day 7 after transplantation. In contrast, one of three FK506-treated recipients showed mild rejection and in the other two thirds a moderate rejection was observed. All β-SQAG9-treated recipients had moderate rejection, suggesting that its suppressive effects were slightly weaker than those of FK506. Interestingly, the number of CD4 T cells in the graft area of β-SQAG9-treated recipients decreased significantly in comparison with control group. These data suggested that β-SQAG9 has promising potential as an immunosuppressant.

Key words: β-SQAG9, immunosuppressant, glycolipid, skin allograft, swine

Introduction

Immunosuppressive agents in clinical use now have some side effects, especially in the kidneys, and therefore the development of new immunosuppressants with specific immunosuppressive effects and few side effects is important for patients who used organ transplantations. To reduce this adverse effect, it may be better to use them in low doses in combination with several other drugs that each has a different activity. For example, FYT720 is known to decrease the number of circulating mature lymphocytes by acceleration of lymphocyte homing (1), and combination treatment with CsA and FYT720 resulted in successful allografted-organ survival (2-4). Therefore, it is important to develop new drugs which are capable of promoting immunosuppressive activity through novel mechanisms.

We previously reported that synthetic sulfonolipid;3-O-(6-deoxy-6 sulfono-β-D-glucopyranosyl)-1,2-di-O-acylglycerol (β-SQDG(18:0)), which is deduced from sulfonoquinovosyl diacylglycerols of sea urchin, has an immunosuppressive effect in vitro and in vivo, and that the immunosuppressive effect is caused by contact inhibition between T cells and antigen presenting cells (APCs) (5,6). Moreover, it was found that β-SQAG9 binds specifically to L-selectin (CD62L) on the T cell surface, which is essential for suppressive effects on human mixed lymphocyte reaction (MLR) in vitro (7). To make clear the effect of β-SQAG9 on animal model that is more closed to human, we here examined the

immunosuppressive effect of β-SQAG9 through swine allogeneic skin grafting as a model.

Materials and Methods

Animals

Hybrid pigs weighing approximately were purchased from Hokudo Co., Ltd, and were bred within the Animal Research Center of Sapporo Medical University. All procedures were performed in compliance with the guidelines of the Animal Research Center of Sapporo Medical University. Nine pigs were equally divided into three groups: a control group, the FK506 group and the β-SQAG9 group. Also, three hybrid pigs were used as donors.

Swine allogeneic MLR

Peripheral blood mononuclear cells (PBMCs) from one donor as stimulator cells, namely antigen processing cells (APCs), were prepared by radiation treatment with 30 gray. PBMCs from another donor as responder cells were incubated on a nylon wool column (Biotest AG, Dreieich, Germany) for 1 h at 37°C in 5% CO_2. T cells that did not bind to the nylon column were suspended with medium. Responder T cells and APCs were mixed at a 1:1 ratio with or without β-SQAG9 or FK506 in RPMI1640 (Nissui Co., Tokyo, Japan) supplemented with 25 mM HEPES, 100 U/ml penicillinG, 100 mg/ml streptomycin, and 10% FCS at 10^6 cells/ml

and aliquoted into triplicate wells of a 96 well round-bottom plate (200 ml/well). After 5 days of cultivation, [^{3}H]thymidine was added to the wells and subsequently cultured for 24 h, and the cells were then harvested with a Filtermate harvester (Packerd, Meriden, CT). [^{3}H]thymidine incorporation was measured on a Topcount NXT microscintilation counter (Packerd, Meriden, CT).

Skin Graft

We anesthetized donor pigs with 15mg/kg ketamine (Sankyo Co., ltd, Tokyo) injected into muscles and inhalation of isoflurane (Dainippon Sumitomo Pharmaceutical Co., Ltd, Osaka) and took split thickness skin from their back and cut the skin into 5cm square pieces. Then, these skin pieces were grafted onto the back skin-defected area of the recipients. One piece of autologous skin was grafted beside to compare with allogeneic skin pieces. FK506 was kindly provided by Fujisawa Pharmaceutical Co., Ltd. β-SQAG9 or FK506 was administered intravenously daily at a concentration of 50mg/kg or 0.1mg/kg in 200ml serine, respectively, for 7 days after the transplantation. The control group was administered only 200ml serine in the same manner. Biopsies were performed on days 4, 7, 10 and 14 after skin grafting, and specimens were frozen and fixed with formalin.

Histological evaluation

For microscopic examination, subdivided tissue was fixed in 10% formalin, processed routinely by embedding in paraffin, and stained with hematoxylin and eosin (HE). All specimens were evaluated and categorized as follows: Grade 1 was mild rejection (intraepidermal spongiosis and blister formation), Grade 2 was moderate rejection (incomplete epidermal separation) and Grade 3 was complete rejection (complete epidermal separation), as we described previously (5, 6). Frozen specimens were stained with anti-porcine CD4α chain or anti-porcine CD8α chain monoclonal antibody (mAb) (Serotec Ltd, Oxford), and were examined by light microscope.

Results and Discussion

Swine allogeneic MLR

We tested whether β-SQAG9 suppressed swine T cell response against allogeneic stimulator. As shown in figure 1, FK506 treatment inhibited swine T cell responses to MLR, and β-SQAG9 inhibited T cell responses in dose dependent manner. These data suggested that β-SQAG9 could also inhibit swine T cell responses to MLR, as was the case in rat and human (5-7). We previously reported that $CD62L^+$, CD4 T cells, by occupying more than 45% of the peripheral blood, predominantly respond to APCs in human MLR (7). Moreover, β-SQAG9 specifically bound to CD62L molecules on the human T cell surface, which could

explain why T cell tolerances were elicited. In this study, since a swine T cell purification system and anti-swine CD62L (L-selectin) antibody were not available, it was not clear which subset of swine T cells predominantly responded to APCs. Further investigations into this matter should prove interesting.

Swine skin allograft

Figure 2 shows gross and histological characteristics of grafted skin of control, FK506, and β-SQAG9 treated recipient on day 7 after transplantation. Since all grafted skins in the control group were judged to be grade 3 rejection (complete rejection) by histological criteria on day 7 after transplantation (figure 2d), we evaluated the histological criteria of biopsy specimens at 7 day. In the FK506 group, gross observations revealed no necrotic site in the grafted skin (figure 2b) when compared with the autograft, and one of three grafts was judged to be grade1 rejection (mild rejection) (figure 2e) and the others were grade 2 rejection by histological examination. In the β-SQAG9 group, gross observations also revealed no necrotic site in the grafted skin (figure 2c) when compared with the autograft, and all 3 grafts were judged to be grade 2 rejection (moderate rejection) by histological examination (figure 2f). In the rat skin allograft study, we previously reported that five of eleven rats (45.5%) were grade 1 rejection and the others (54.5%) were grade 2 rejection (6). Compared with